Automated Response Matching for Organic Scintillation Detector Arrays

M.D. Aspinall, M.J. Joyce, F.D. Cave, R. Plenteda, A. Tomanin

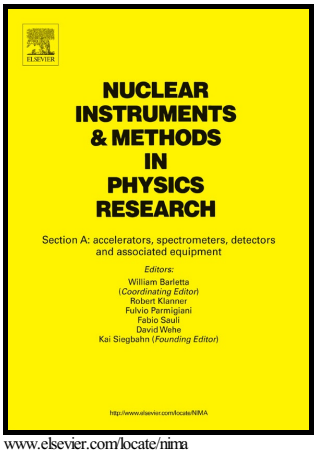

www.elsevier.com/locate/nima

PII: S0168-9002(17)30533-8
DOI: http://dx.doi.org/10.1016/j.nima.2017.05.004
Reference: NIMA59842

To appear in: *Nuclear Inst. and Methods in Physics Research, A*

Received date: 12 November 2016
Revised date: 3 May 2017
Accepted date: 4 May 2017

Cite this article as: M.D. Aspinall, M.J. Joyce, F.D. Cave, R. Plenteda and A Tomanin, Automated Response Matching for Organic Scintillation Detecto Arrays, *Nuclear Inst. and Methods in Physics Research, A* http://dx.doi.org/10.1016/j.nima.2017.05.004

Automated Response Matching for Organic Scintillation Detector Arrays

M.D. Aspinall[a,*], M.J. Joyce[a], F.D. Cave[b], R. Plenteda[c], A. Tomanin[c]

[a] *Department of Engineering, Lancaster University, Bailrigg, Lancaster, Lancashire, LA1 4YR, UK*
[b] *Hybrid Instruments Ltd., Lancaster Environment Centre, Lancaster University, Bailrigg, Lancaster, Lancashire, LA1 4YW, UK*
[c] *International Atomic Energy Agency (IAEA), Vienna International Centre, PO Box 100, A-1400 Vienna, Austria*

Abstract

This paper identifies a digitizer technology with unique features that facilitates feedback control for the realization of a software-based technique for automatically calibrating detector responses. Three such auto-calibration techniques have been developed and are described along with an explanation of the main configuration settings and potential pitfalls. Automating this process increases repeatability, simplifies user operation, enables remote and periodic system calibration where consistency across detectors' responses are critical.

Keywords: Detector response matching, real time systems, fast neutron detection, radiation monitoring, spectroscopy, digital signal processing.

1. Introduction

Large scintillation detector arrays and multi-channel digitizers have reported use for the assay of radiation fields associated with fast neutrons [1–11]. However, shortcomings of photo-multiplier tube (PMT) technology that scintillation detectors rely means similar detectors with the same hardware arrangement and supply bias do not produce comparable responses. Significant PMT variances and other environmental instabilities must be accounted for in measurements

*Proofs author. Tel: +44 743 600 9071
Email address: m.aspinall@lancaster.ac.uk (M.D. Aspinall)

that depend on matched detector performance. Consequently, supply biases are usually adjusted manually and individually to control PMT gain and match the detectors' responses.

In addition, multi-channel, fast digitizers are the choice of data acquisition (DAQ) electronics for the signals derived from these detectors. Sampling frequencies of greater that 250 MSa/s are typically required of these digitizers given that the pulses to be digitized have widths of the order of tens of nanoseconds and adequate pulse information is necessary for pulse shape discrimination (PSD), among other analyses.

The maturity of these two technologies, their ability to detect fast neutrons directly, perform neutron/gamma discrimination reliably and low dead-time have made them a popular choice for helium-3 alternatives [1], enhanced nuclear safeguards and security monitoring [2–9] and fast neutron imaging applications [10, 11]. Besides the choice of detector and DAQ, all these measurements analyse data from multiple detectors. Detector arrays of this sort can range from a pair of detectors to arrays consisting of tens of detectors.

Fast neutron scintillation detectors rely predominately on established photomultiplier tube (PMT) technology for scintillation light output capture, photon-to-charge conversion and charge amplification. The PMT gain can have significant variance as a result of the multiplication of the tolerances associated with the resistors used in the dynode chain (the tolerance of a resistor is the deviation that a resistor may vary from its nominal value resistance, measured at 25°C with no load applied).

Furthermore, these carbon-based resistances cause PMT technology to have temperature dependence of sensitivity and response. Consequently, detector response functions can vary due to changes in the ambient environment and can vary greatly from one detector to another [12]. Subsequently, some detector arrays, where the balance of detection response is of paramount importance, have been commissioned with high tolerances and with a built-in trim resistor on the PMT for gain adjustment, here, at best only a tolerance of ±10% could be assured by the manufacturer [13].

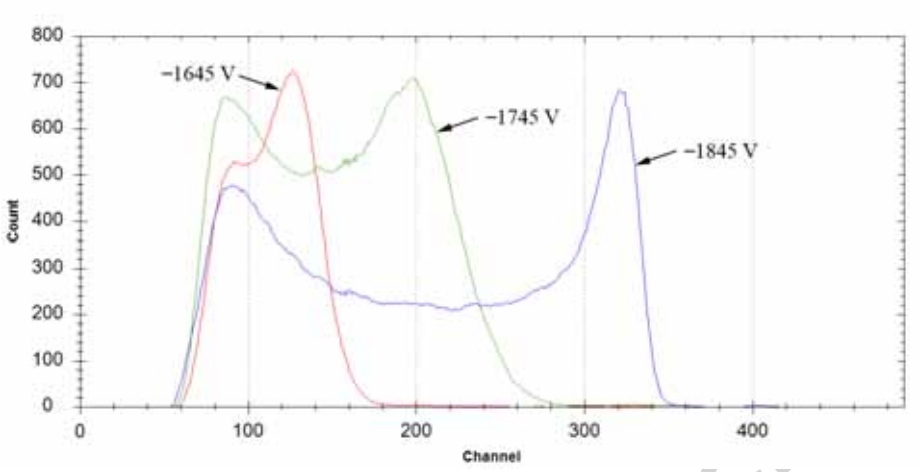

Figure 1: Cs-137 spectra with 10-point finite impulse response (FIR) filter acquired from an EJ309 liquid scintillator operated with a negative bias of 1645 V, 1745 V and 1845 V. This illustrates the effect different PMT biases have on the pulse height spectra, particularly the location of the Compton edge.

The nature of any mixed-field analysis using an organic scintillation detector array (or indeed any combination of sensors where the amplification stages are vulnerable to changes in gain or HV setting) relies on the comparison of count rate and derived parameters such as spectra, neutron/gamma ratio, coincidence, multiplicity, or a combination. Even with a base-line measurement across the array the nonlinear response curves inhibit the potential to extract practical data, hence matching the response functions of all detectors in the array is essential to any meaningful interpretation of data.

By adjusting the supplied high voltage (HV) the pulse height spectra (PHS), used as a measure of PMT gain, can be compressed or elongated as is illustrated by the Cs-137 PHS shown in Fig. 1. Detectors are response matched, in these instances, by aligning the Compton edge observed on the PHS of Cs-137 from multiple detectors. For arrays with a significant number of individual detectors it is time consuming for the operator to manually adjust the HV for every detector to match responses based on the PHS. Furthermore, manual configuration is prone to human errors that reduce repeatability and consistency of setup.

Detectors that are response matched can standardize hardware parameters (e.g. pre-amplifier, trigger threshold and PSD metrics), this alone can reduce setup time by not having to determine and apply different settings across several different detector channels and also generalizes the setting for use with comparable system setups. Similarly, for universal PSD parameters to be applicable across a detector array, detectors must have similar characteristics, response functions and sensitivities [7]. In the past, this has been achieved by monitoring the detector count rates, visually inspecting the PSD scatter plots and neutron/gamma ratios derived from measurements with a Cf-252 source [4, 13] (NB. PHS analysis was unavailable in this instance). Traditionally, individual detector responses have had to be manually altered either using the trim potentiometer on the PMT or the supplied HV or both. However, in the majority of cases a PMT trim potentiometer may not be available or accessible and all response matching is limited to adjusting the HV supply.

Automating this process increases the repeatability of measurements, simplifies the user operation and reduces the time taken to match the responses of detectors by manually adjusting the HV. Furthermore, it removes the reliance on the operator's visual interpretation of the PHS to determine a suitable PMT bias. The automation of this process also enables remote and periodic system calibration where the accuracy of the measurement is critical and there exists a significant environmental gradient across the detector array.

The significant variance of PMT gain means fast neutron assay utilizing scintillation detectors would benefit from controllable HV supplies that are integrated with the digital acquisition electronics. A hardware arrangement of this sort affords control of PMT gain with feedback and is necessary for automating the process of response-matching using software algorithms that determine the detector's response and adjusts the HV accordingly. This paper reports on the development and testing of three such algorithms referred herein as autocalibration methods.

Figure 2: The front panel of the quad-channel Mixed-Field Analyzer (model no. MFAx4.3). Source: http://www.hybridinstruments.com

2. The Enabling Technology

The auto-calibration methods discussed are made possible because of three key features of the Mixed-Field Analyzer (model no. MFAx4.3) hardware by Hybrid Instrument Ltd., UK. The MFAx4.3 is a quad-channel high-speed digitizer designed specifically to perform PSD on events arising from fast scintillators in real-time. A comprehensive review of the current status of the MFA technology shown in Fig. 2 is reported [14]. In brief and for the purpose of this paper, the three features of the technology that enable the methods discussed are summarized.

1. The MFA hardware supports Ethernet connectivity for direct PC interface and use of a graphical user interface (GUI) software environment to afford system diagnostics and setup.
2. The hardware can be configured from the GUI to stream either PSD data or pulse height data to the host PC. When configured to multi-channel analyzer (MCA) mode the software automatically configures to display MCA windows to report PHS.

3. The embedded/integrated HV supplies (one dedicated per high-speed digital input channel) means that the individual detector HV supplies can be controlled from the same GUI used for data analysis.

This combination of PC-based control interface, real-time pulse height analysis and embedded HV supplies means that the real-time PHS can be analyzed by the software and used as feedback to automatically match detector responses by adjusting the supplied HV.

3. The Implemented Auto-Calibration Methods

The software-based, real-time auto-calibration methods discussed in this paper were developed in partnership between Lancaster University, Hybrid Instruments Ltd. and the IAEA. The auto-calibration methods were embedded into Hybrid's interface software for use with their MFA hardware suite.

3.1. MCA Settings

From the calibration window of the GUI the user is able to specify all settings for the MCA and auto-calibration. Fig. 3 shows where all the MCA and auto-calibration settings are located in the GUI configuration window (the following numbers in superscript correspond to the setting highlight in Fig. 3). Here it is possible to specify the number of channels contained in the MCA (*number of MCA channels*[1]), the maximum signal peak amplitude represented on the MCA (*Maximum peak*[2]) and the amount of filtering applied to the PHS (*MCA FIR filter*[3]), the latter of which will be discussed later. The *Maximum peak* setting on the MCA stops oversized events that have saturated the input from populating the rightest channels of the MCA. Events of this sort would be most prevalent when the applied bias to the PMT and hence PMT gain is set too high relative to the dynamic range on the digital input (which is governed somewhat by the pre-amplifier gain and fixed hardware capabilities), resulting in pulses that have amplitudes larger than can be digitized.

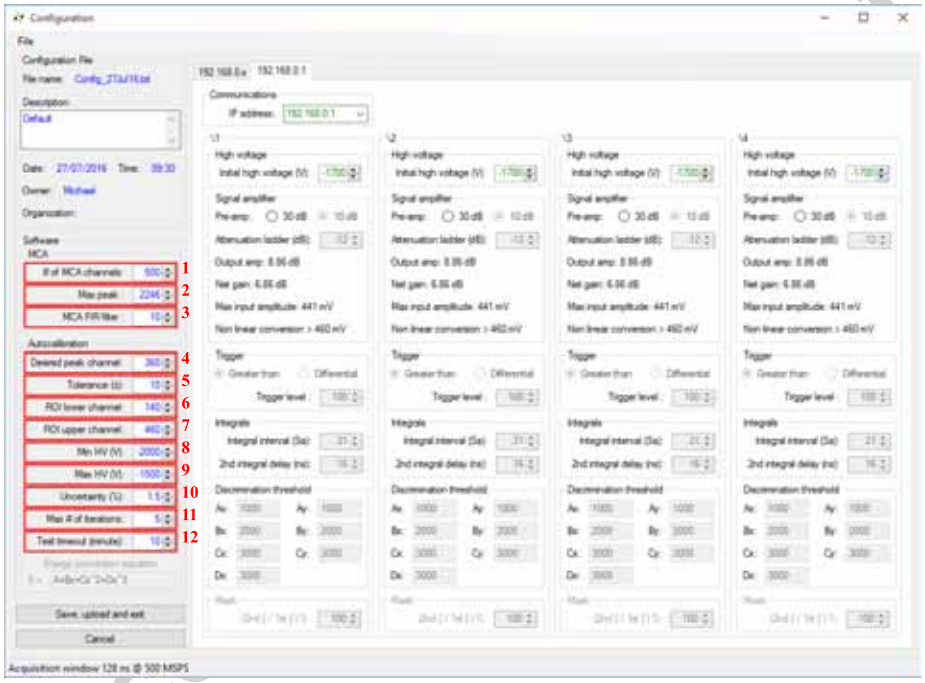

Figure 3: A screen capture of the GUI configuration window with the MAC and auto-calibration settings highlighted and corresponding to the labelled PHS shown in Fig. 4.

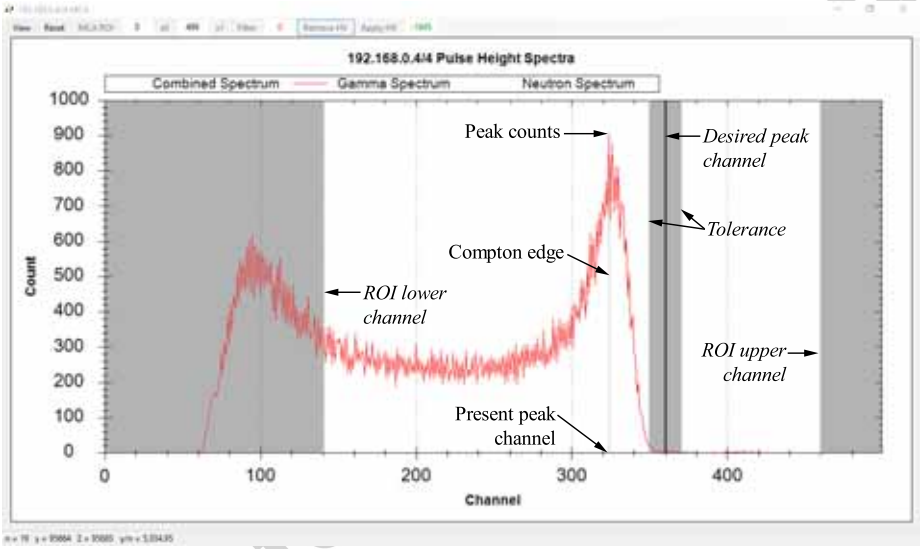

Figure 4: Cs-137 pulse-height spectrum acquired from an EJ309 liquid scintillator operated with a negative bias of 1845 V, the present peak channel (the peak of the Compton edge) is located at channel 324. The desired peak channel, in this instance, is channel 360 with a tolerance of ± 10 channels. The ROI lower channel is located at channel 140 and the ROI upper channel is located at channel 460.

3.2. Auto-Calibration Settings

All techniques described rely on modelling the relationship between the MCA channel number that contains the maximum counts in the Compton edge region of a Cs-137 PHS (referred to as *peak channel*) and the HV supplied to the PMT. The implemented algorithms use a combination of the previous peak channel, current peak channel, previous HV and current HV to determine the next HV setting in an attempt to align the peak channel with the *desired peak channel*[4]. For the convenience of this paper these are referred to as *past* (for previous settings, both peak channel and HV), *present* (for current settings, both peak channel and HV) and *future* (for the new setting, HV only).

The MCA data is represented in software as an array of integers, each element of the 1-D array represents a single channel of the MCA, therefore the total number of array elements defines the total number of MCA channels. The present peak channel is determined by passing each element of the array through a loop that tests for maximum counts. Limits are defined to reduce the number of array elements to test and therefore reduce the processing time and to avoid finding the peak channel in the region to the far left of the Compton edge. These limits are referred to as *ROI lower channel*[6] and *ROI upper channel*[7] and are specified by the user in the GUI.

The user also specifies the *desired peak channel* of the Compton edge on the MCA and the allowable *tolerance*[5] on this channel number. These user settings are represented visually in Fig 4 of a typical Cs-137 PHS from an EJ309 liquid scintillator acquired using the interface software configured in MCA mode. The number of counts to be acquired in the peak channel is determined by the percentage *uncertainty*[10], where the number of counts = $(100/uncertainty)^2$, as derived from the fractional uncertainty $1/\sqrt{counts}$.

To protect the detector and PMT from over voltage damage a minimum allowable HV is specified. Slightly misleadingly, the *minimum HV*[8] is the maximum absolute value because the HV is negative. Similarly, the *maximum HV*[9] is the minimum absolute value and prevents a bias being set that is too insignificant to drive the detector and obtain sufficient data.

Two other settings, *max number of iterations*[11] and *test timeout (minutes)*[12], are used to limit the maximum possible time spent attempting auto-calibration. If the number of attempts to calibrate a channel exceeds the *max number of iterations* the calibration of that channel is terminated. The calibration of all channels is terminated if the total runtime exceeds the specified *test timeout (minutes)*.

There is potential for calibration of a single or all channels to fail and is typically due to poor choice of user configuration settings. Table 1 presents auto-calibration report messages, a probable cause of failed calibration and an explanation.

3.3. Initialization and General Conditions

During the initialization of the auto-calibration procedure the system automatically switches to MCA mode if not already in that mode, all open plot windows are closed and all arrays are cleared of previously processed data. The apply-to-all option on the HV setting is unchecked given that different HV settings will certainly exist across calibrated channels. Finally, an auto-calibration start time is recorded.

In all three methods three states exist in relation to the present peak channel and the desired peak channel. These states are listed below and are referenced during the explanation of each of the auto-calibration methods.

S1) The present peak channel is greater than *desired peak channel* + *tolerance* (i.e. absolute value of the HV is too great).

S2) The present peak channel is less than *desired peak channel* − *tolerance* (i.e. absolute value of the HV is too low).

S3) The present peak channel is equal to the *desired peak channel* ± *tolerance* (i.e. the HV is acceptable).

3.4. Linear Fit Method

With this method channels are calibrated sequentially. All HVs are first switched off, one HV channel is switched on at a time, calibrated and then

Report Message	Probable Cause	Explanation
FAIL: {device IP address}/{channel #}. HV attempt out of range. HV set to 0 V, manual configuration required.	Range of allowable HVs are set too narrow.	Calculated future HV falls outside the allowable range of HVs. Calibration of this channel will be terminated.
FAIL: {device IP address}/{channel #}. HV attempt out of range. HV set to 0 V, manual configuration required.	ROI lower channel is set too low.	Peak channel of left-hand peak assumed to be that of the Compton edge region. Using incorrect peak channel to calculated future HV will likely cause it to exceed the allowable range of HVs. Calibration of this channel will be terminated.
FAIL: {device IP address}/{channel #}. Maximum iterations reached. HV set to 0 V, manual configuration required.	Max number of iterations is set too low.†	Inappropriate expectation of the number of iterations required to successfully calibrate a channel relative to other constraints. Calibration of this channel will be terminated.
FAIL: Auto-calibration timed-out. Manual configuration required on remaining channels.	Test timeout (minutes) is set too low.‡	Inappropriate expectation of the time required to successfully calibrate all channels relative to other constraints. Calibration of remaining uncalibrated channels will be terminated.
SUCCESS: {device IP address}/{channel #}. HV set to {volts} V, peak channel at {peak channel}.	n/a	Calibration of this channel was successful. The calibrated HV value and corresponding peak channel are reported.

Table 1: Typical auto-calibration report messages, probable cause of failure and brief explanation.

† Relative to a). the tolerance on the desired peak channel and b). the number of MCA channels. These settings have an impact on the number of iterations to calibrate a channel and should be considered when optimizing the MCA and auto-calibration settings.

‡ Relative to a). the tolerance on the desired peak channel, b). the number of MCA channels, c). the number of channels between the ROI lower and ROI upper channel (i.e. the number of channels tested for maximum counts), d). the amount of filtering applied to the PHS and e). the activity and proximity of the calibration source. All these settings have an impact on the auto-calibration processing time and should be considered when optimizing the MCA settings, auto-calibration settings and geometry of the experimental setup.

switched off before moving on to the next channel. This is to stop high-rate channels from consuming the processing bandwidth and preventing other channels from calibrating. When complete all calibrated HVs are switched back on.

Once the statistical uncertainty has been met in the peak channel for the first time (i.e. past HV and past peak channel are NOT available) the present peak channel and present HV are used to calculate the future HV based on the assumption that the relationship between peak channel and absolute HV is directly proportional and passes through the origin (i.e. y-intercept equal to zero).

If it is not the first iteration (i.e. past HV and past peak channel are available) then in both cases the future HV is calculated on the basis that the relationship between the peak channel and absolute HV is directly proportional. The gradient and y-intercept are derived from the past peak channel, the present peak channel, the past HV and present HV, effectively dy/dx. The gradient and y-intercept of this linear relationship are then used with the desired peak channel to calculate the future HV. Past and present variables are reassigned accordingly, the new HV is set and the process continues until state S3 is met, or the maximum number of iterations is reached, or an attempt to set an out-of-range HV, or the entire process times-out.

Once state S3 is met the HV on that channel is set to zero, the subsequent channel's HV is switched on and the calibration process repeated.

3.5. Binary Search Method

This method also calibrates channels sequentially and implements a simple binary search algorithm to do so. The initial HV is determined by calculating the mid-point value between the user specified maximum and minimum HVs. Once the statistical uncertainty has been met the present peak channel is compared to the desired peak channel, if state S1 is true the HV value at the mid-point between the present HV and the lower value of the absolute HV (i.e. the maximum HV) is the next HV applied. Conversely, if state S2 is met the

HV value at the mid-point between the present HV and the greater value of the absolute HV (i.e. the minimum HV) is the next HV setting. This process is repeated until state S3 is true, or the maximum number of iterations is reached, or the entire process times out.

With this method the calibrated HV is achieved in no more than ($\log_2$ N) iterations (rounded-up to the nearest integer), where N is the number of potential MCA channels for the peak channel. Using Fig. 4 for example, an MCA with 500 channels, the desired peak channel may only be possible in 1 of 320 of the channels because of the ROI lower channel (140) and ROI upper channel (460) limits. This being the case ($\log_2$ 320) = 8.3, therefore, the calibrated HV should be achieved in 9 or less iterations (i.e. the minimum number of bits needed to represent 320, $2^9 = 512$). This is often an over estimation because of leniencies introduced by the tolerance on the desired peak channel.

The simplicity of this method means that no previous HV setting is used as a starting point when auto-calibration is evoked, instead the HV first applied is always the mid-point value between the user specified maximum and minimum HVs.

3.6. Optimized Linear Fit Method

Unlike the previous two, this method attempts to calibrate channels simultaneously by processing data from all active channels in parallel. After a channel has been calibrated the HV is switched off to reduce the volume of data being processed and reduce the time taken to calibrate the remaining uncalibrated channels. When calibration is complete all calibrated HVs are switched back on.

Once the statistical uncertainty has been met in the peak channel for the first time (i.e. past HV and past peak channel are NOT available) the present peak channel is compared to the desired peak channel. If the state is S1 the future HV is simply equal to (present HV − 20). Similarly, if state S2 the future HV is equal to (present HV + 20).

Similar to the standard linear fit method, if it is not the first iteration then in

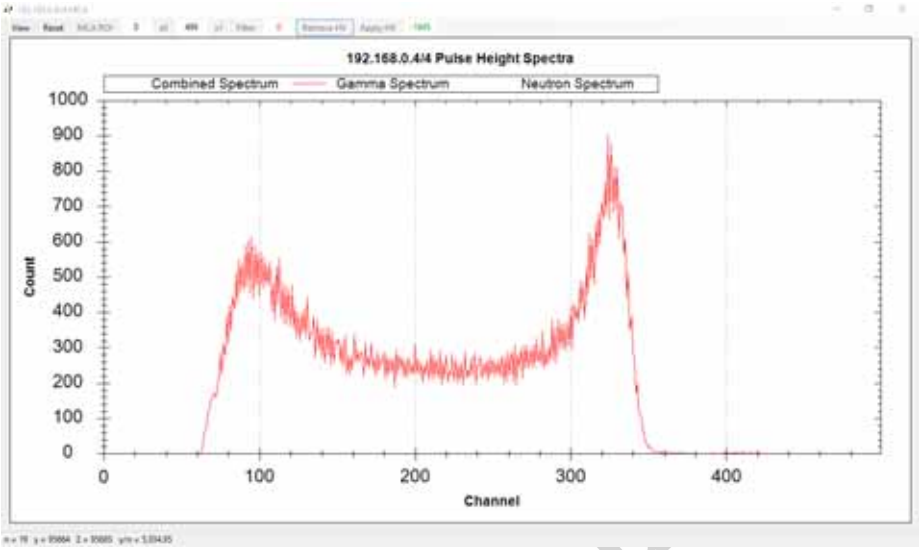

(a)

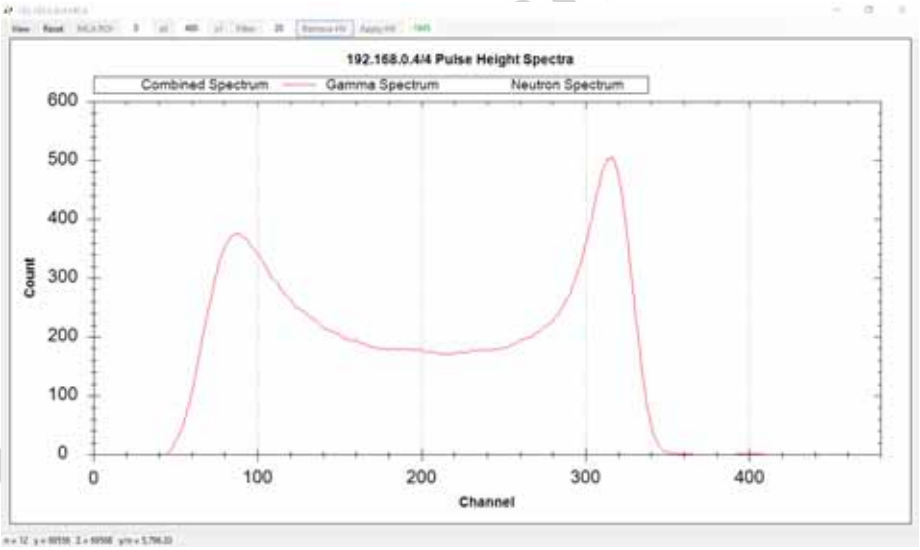

(b)

Figure 5: The multi-channel analyzer (MCA) graphical-interface with unfiltered gamma-only pulse-height spectrum 5a and with 20-point finite impulse response (FIR) filtered gamma-only pulse-height spectrum 5b of data acquired from an EJ309 liquid scintillator positioned 45 mm from a Cs-137 source.

both cases the future HV is calculated on the basis that the relationship between the peak channel and absolute HV is directly proportional. The gradient and y-intercept are derived from the past peak channel, the present peak channels, the past HV and present HV, as before and used with the desired peak channel to calculate the future HV. Past and present variables are reassigned accordingly, the new HV is set and the process continues until state S3 is met, or the maximum number of iterations is reached, or an attempt to set an out-of-range HV, or the entire process times out.

Another improvement of this method is the implementation of a real-time embodiment of a finite impulse response (FIR) filter for MCA data. The smoothing effect that this has on the PHS is very beneficial, for both human and computational interpretation, in better determining the peak channel in the Compton edge. The magnitude of the filter can be set whilst acquiring data and the filtering influence displayed in real time. *MCA FIR filter* is a user specified requirement of the MCA settings as detailed in section 3.1. Fig. 5 shows an unfiltered PHS and a 20-point FIR filtered PHS for Cs-137 acquired from an EJ309 liquid scintillator. This filtering improves the reliability by which the software algorithm can determine the peak channel in the Compton edge region.

4. Results and Discussion

The linear fit method showed promise, however, assuming that the linear relationship between peak channel and HV passes through the origin for the first iteration is an unsuitable model. This model occasionally caused calculated HVs to continuously alternate between either being too high or too low, never allowing the channel to calibrate. This was particularly prominent when the initial HV was far from the HV setting actually required to achieve the desired peak channel.

The binary search method was significantly more reliable than the linear fit method. However, this implementation is inefficient given that all prior HV settings are discarded and even if an original HV matched the criteria it

would still pass through a full calibration procedure and take, up to as many as, $(\log_2 N)$ iterations, where N is the number of channels tested for maximum counts. This drastically increased the time required to complete auto-calibration especially for considerably large arrays and calibration sources with particularly low activity.

The optimized linear fit method rectified the issues highlighted with the original linear fit method by calculating a gradient and y-intercept of the initial HV for the first iteration using a small ± 20 V change in the initial HV. This produced a closer linear model of the non-linear relationship between the peak channel and HV and on average required about four iterations.

Fig. 6 shows calibrated PHS from four EJ309 liquid scintillators using the optimized linear fit method and a 331 kBq Cs-137 calibration source. Fig. 7 shows the PSD scatter plots for the same four calibrated detectors exposed to the Cs-137 source. The four detectors were positioned with the edges of their front faces touching to form a 100 mm square, the source was placed in the centre of the four detectors. The MCA was configured with 500 channels, the desired peak channel was set to channel 250 ± 10 and the PHS were smoothed with a 30-point FIR filter. The uncertainty was set to 5%, equating to 400 counts ($(100/5)^2$) in the peak channel of the Compton edge. The ROI lower channel was set to 200 and the ROI upper channel was set to 499. For this particular set-up and source activity the auto-calibration took about 4 minutes to complete, the notifications reported during the process are shown in Fig. 8.

The speed that the system and the described methods can automatically calibrate a detector depends on several variables. Table 2 details these variables together with an explanation of how it affects the rate of pulse-height data acquisition and computer processing time and ultimately the speed of auto-calibration. The variables have been ordered by how easily they can be altered and the significance that they have on the speed of auto-calibration.

Filtering the PHS produced smoother spectra that made the identification of the peak channel more reliable. For instance, with the previous two methods the peak channel could potentially shift with significant impact (i.e. fall outside

System Variable	Slows Down Auto-calibration	Speeds Up Auto-calibration
Proximity of the source to the detector (hardware; easily adjusted providing no physical constraints exist)	Greater distance of the source from the detector will take more time to acquire the specified statistical uncertainty in the peak of the Compton edge and will require a relatively long test timeout period.	Shorter distance of the source from the detector will take less time to acquire the specified statistical uncertainty in the peak of the Compton edge and will not require as long a test timeout period.
Detector trigger threshold (software /firmware; easily adjusted using the calibration GUI)	Lower trigger thresholds will process a relatively high rate and range of pulse heights with a lower proportion of these pulses being in the useful Compton edge region. This will take more time to acquire the specified statistical uncertainty in the peak of the Compton edge and will require a relatively long test timeout period.	Greater trigger thresholds will process a relatively low range of pulse heights with a greater proportion of these pulses being in the useful Compton edge region (providing the threshold is not so great that peak of the Compton edge is not discarded). This will take less time to acquire the specified statistical uncertainty in the peak of the Compton edge and will not require as long a test timeout period.
Calibration source activity (hardware; depends on source availability)	Low activity will take more time to acquire the specified statistical uncertainty in the peak of the Compton edge and will require a relatively long test timeout period.	High activity will take less time to acquire the specified statistical uncertainty in the peak of the Compton edge and will not require as long a test timeout period.
Detector efficiency (hardware; fixed and would require detector redesign)	Lower detector efficiency will take more time to acquire the specified statistical uncertainty in the peak of the Compton edge and will require a relatively long test timeout period.	Higher detector efficiency will take less time to acquire the specified statistical uncertainty in the peak of the Compton edge and will not require as long a test timeout period.
Detector volume (hardware; fixed and would require detector redesign)	Smaller detector volumes will take more time to acquire the specified statistical uncertainty in the peak of the Compton edge and will require a relatively long test timeout period.	Larger detector volumes will take less time to acquire the specified statistical uncertainty in the peak of the Compton edge and will not require as long a test timeout period, but may have reduced PSD quality.
ROI lower channel and upper channel range (software; easily adjusted using the calibration GUI)	Wide range will take more time to find the present peak channel, will increases the risk of finding the left-hand (scatter) peak on the MCA and may attempt to locate this to the desired peak channel.	Narrow range will take less time to find the present peak channel, but will increases the risk of the envelope not encompassing the peak of the Compton edge and therefore not finding the true location of the present peak channel on the MCA.

Table 2: System variables with an influencing factor on the speed that the system and the described methods can automatically calibrate a detector.

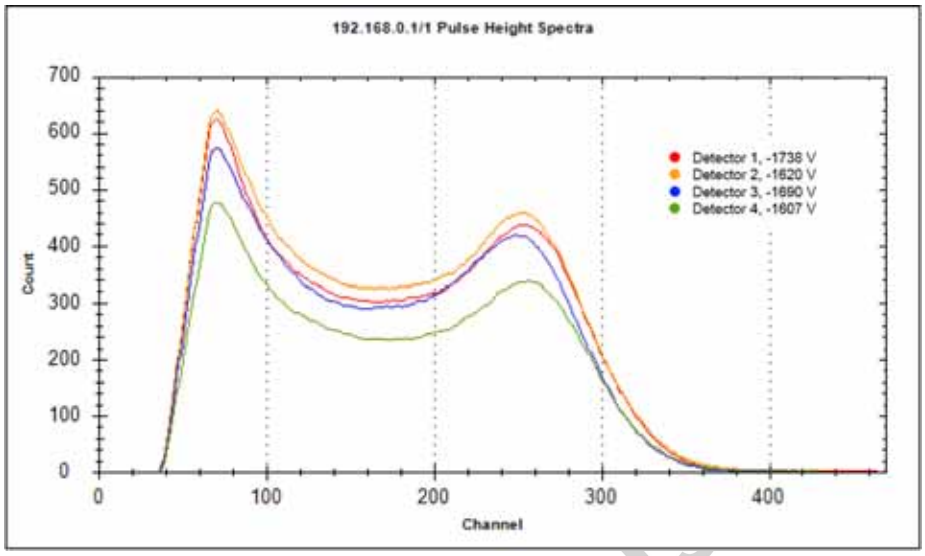

Figure 6: Superimposed Cs-137 pulse-height spectra from four EJ309 scintillators calibrated using the optimized linear fit method. The MCA was configured with 500 channels, the PHS was smoothed with a 30-point FIR filter, the desired peak channel was set to channel 250 ± 10.

of the *desired peak channel* ± *tolerance*) simply because of Poisson fluctuations seen in the unfiltered spectrum shown in Fig. 5a. The improved spectrum, filtered using a 20-point FIR, is shown in Fig. 5b. However, currently the MFA hardware, when configured in MCA, reports a single sample to represent the pulse height. By summing multiple samples around the peak of the pulse (the method used by most multi-channel analyzers) the resolution of the pulse height would be improved and the tolerance to signal noise would be better potentially reducing the reliance on the PHS filter.

The optimized linear fit method reduced calibration time by performing data capture and analysis in parallel across all uncalibrated channels instead of calibrating channels sequentially as with the earlier two methods. However, when a new HV is calculated and updated, all HVs of the MFA are switch off and then switch back on and ramped up to the existing HVs bar the newly calculated HV which replaces its existing. This regular cycle of switching off all

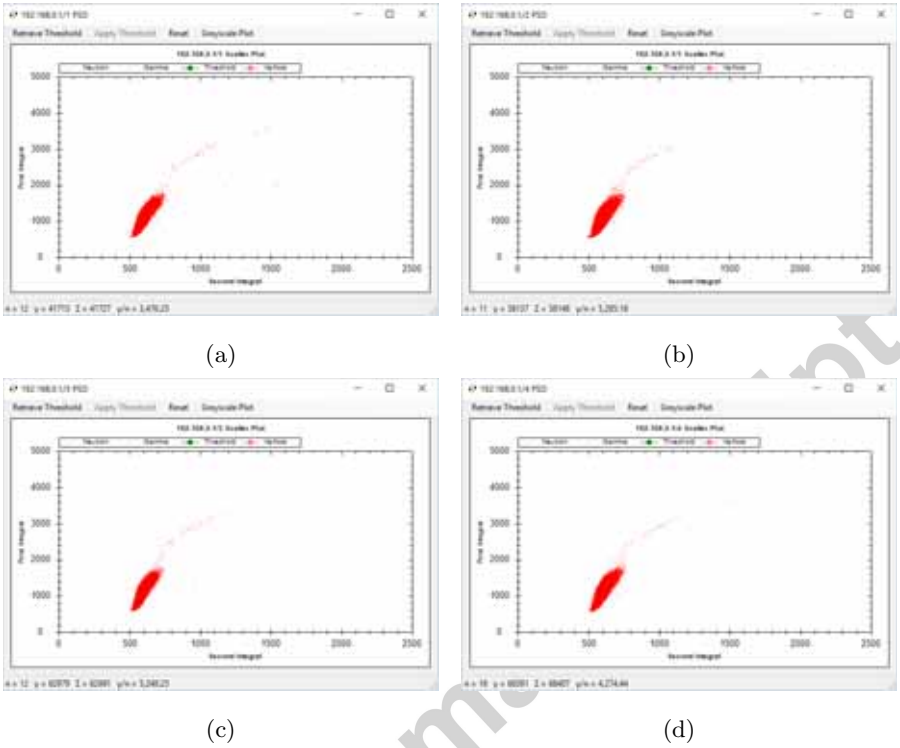

(a) (b)

(c) (d)

Figure 7: Cs-137 PSD scatter plots for four EJ309 scintillators calibrated using the optimized linear fit method. Each plot shows the gamma plume recorded with a Cs-137 source placed on-axis and 50 mm from the front face of the detectors.

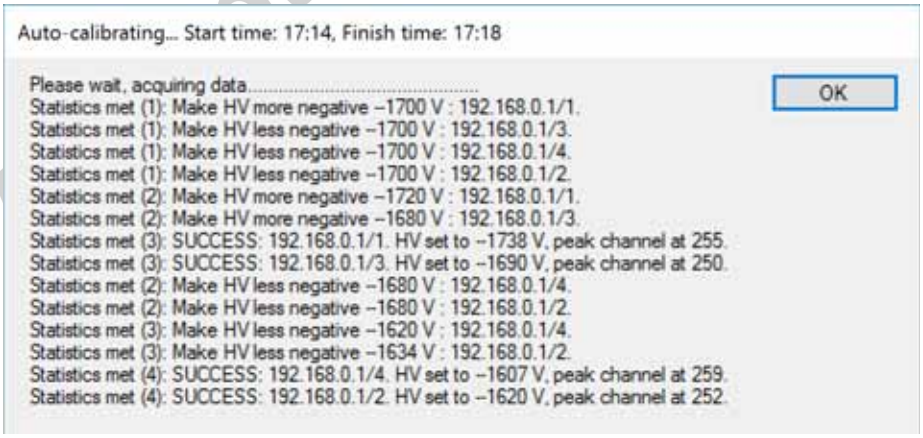

Figure 8: Notifications reported during the optimized linear method for the superimposed Cs-137 pulse-height spectra shown in Fig. 6 and the PSD scatter plots shown in Fig. 7.

HVs to update the HV on just one of those channels is not optimal and influences the distribution of pulse heights recorded during the ramping up of the HVs. Consequently, this contributes to the PHS recorded and used for determining the appropriate operating HV and so has a detrimental effect on the calibration data.

Initially, the auto-calibration function was designed as a support tool for nuclear inspectors utilizing these systems for nuclear safeguards monitoring and verification. Scintillation detector systems and associated digital processing technology would be taken into the field and require periodic calibration or calibration following transit and system set-up. Automation of the calibration process would speed-up set-up time, improve repeatability and consistency and be operated by an inspector not specifically trained for manual calibration of the system. Nonetheless, this function could also be applied during long measurements to monitor possible gain shifts, especially where environmental changes are prominent and consistency of detector performance is critical to the measurement campaign, providing a characteristic energy peak exists indefinitely in the field under observation.

5. Conclusions

This paper has highlighted the need and benefits of auto-calibration methods for organic scintillation detector arrays. We have reported on the development, implementation and testing of three auto-calibration methods that were employed on a multi-channel digitizer with integrated detector HV supplies. Required MCA and auto-calibration settings have been identified and potential pitfalls of ineffective settings described. Areas of current shortcomings and future developments have also been reported.

Acknowledgment

We thank the IAEA for their contribution and development of some of the techniques described.

References

[1] D. Henzlova, R. Kouzes, R. McElroy, P. Peerani, M. Aspinall, K. Baird, A. Bakel, A. Borella, M. Bourne, L. Bourva, F. Cave, R. Chandra, D. Chernikova, S. Croft, G. Dermody, A. Dougan, J. Ely, E. Fanchini, P. Finocchiaro, V. Gavron, M. Kureta, K. Ianakiev, K. Ishiyama, T. Lee, C. Martin, K. M. Kinny, H. Menlove, C. Orton, A. Pappalardo, B. Pedersen, D. Peranteau, R. Plenteda, S. Pozzi, M. Schear, M. Seya, E. Siciliano, S. Stave, L. Sun, M. Swinhoe, H. Tagziria, J. Takamine, S. Vaccaro, A.-L. Weber, T. Yamaguchi, H. Zhu, Current status of helium-3 alternative technologies for nuclear safeguards, in: National Nuclear Security Administration, U.S. Department of Energy, and The Euratom Atomic Energy Community (Euratom), Ispra, Italy, 2015.

[2] A. Enqvist, K. J. Weinfurther, M. Flaska, S. A. Pozzi, Characterization of a mixed multiplicity counter based on liquid organic scintillators, IEEE Trans. Nucl. Sci. 58 (2011) 2413–2420. doi:10.1109/TNS.2011.2164554.

[3] J. L. Dolan, E. C. Miller, A. C. Kaplan, A. Enqvist, M. Flaska, A. Tomanin, P. Peerani, D. L. Chichester, S. A. Pozzi, Passive measurement of organic-scintillator neutron signatures for nuclear safeguards applications, in: IEEE Nucl. Sci. Symp. and Med. Imag. Conf. (NSS/MIC), Anaheim, CA, 2012. doi:10.1109/NSSMIC.2012.6551093.

[4] M. J. Joyce, K. A. A. Gamage, M. D. Aspinall, F. D. Cave, A. D. Lavietes, A 4-channel multiplex analyzer for real-time, parallel processing of fast scintillators, in: IEEE Nucl. Sci. Symp. and Med. Imag. Conf. (NSS/MIC), Anaheim, CA, 2012, pp. 134–138. doi:10.1109/NSSMIC.2012.6551077.

[5] J. K. Polack, A. Poitrasson-Riviere, M. C. Hamel, K. Ito, S. D. Clarke, M. Flaska, S. A. Pozzi, A. Tomanin, P. Peerani, Image reconstruction of shielded mixed-oxide fuel using a dual-particle imaging system, in: IEEE Nucl. Sci. Symp. and Med. Imag. Conf. (NSS/MIC), Seattle, WA, 2014. doi:10.1109/NSSMIC.2014.7431091.

[6] M. J. Joyce, K. A. A. Gamage, M. D. Aspinall, F. D. Cave, A. D. Lavietes, Real-time, fast neutron coincidence assay of plutonium with a 4-channel multiplexed analyzer and organic scintillators, IEEE Trans. Nucl. Sci. 61 (3) (2014) 1340–1348.

[7] M. J. Joyce, J. Adamczyk, M. D. Aspinall, F. D. Cave, R. Plenteda, Real-time, fast neutron detection for stimulated safeguards assay, in: Proceedings of 37th ESARDA Symp. on Safeguards and Nucl. Non-Proliferation, Manchester, UK, 2015.

[8] H. M. O. Parker, M. D. Aspinall, A. Couture, F. D. Cave, C. Orr, B. Swinson, M. J. Joyce, Active fast neutron singles assay of 235U enrichment in small samples of triuranium octoxide, Progress in Nucl. Energy. 93 (2016) 59–66. doi:10.1016/j.pnucene.2016.07.022.

[9] R. Sarwar, M. J. Joyce, C. H. Zimmerman, Real-time fast-neutron plutonium assay for storage and ageing applications, in: 2nd Annual Meeting DISTINCTIVE University Consortium, Bristol, UK, 2016.

[10] A. Poitrasson-Riviere, M. Flaska, M. C. Hamel, J. K. Polack, M. F. Becchetti, B. M. Wieger, A. Enqvist, S. D. Clarke, S. A. Pozzi, Digital data acquisition and processing for a neutron-gamma-ray imaging system, in: IEEE Nucl. Sci. Symp. and Med. Imag. Conf. (NSS/MIC), Anaheim, CA, 2012. doi:10.1109/NSSMIC.2012.6551381.

[11] M. J. Joyce, S. Agar, M. D. Aspinall, J. S. Beaumont, E. Colley, M. Colling, J. Dykes, P. Kardasopoulos, K. Mitton, Fast neutron tomography with real-time pulse-shape discrimination in organic scintillation detectors, Nucl. Instruments and Methods in Physics Res. A 834 (2016) 36–45. doi:10.1016/j.nima.2016.07.044.

[12] J. B. Birks, The Theory and Practice of Scintillation Counting, Vol. 27, International Series of Monographs on Electronics ad Instrumentation, Pergamon Press, 1964.

[13] A. D. Lavietes, R. Plenteda, N. Mascarenhas, L. M. Cronholm, M. D. Aspinall, M. J. Joyce, A. Tomanin, P. Peerani, Development of a liquid scintillator-based active interrogation system for LEU fuel assemblies, in: IEEE 3rd Int. Conf. on Advancements in Nucl. Instrum. Meas. Methods and their Appl. (ANIMMA), Marseille, France, 2013. doi:10.1109/ANIMMA.2013.6728037.

[14] M. D. Aspinall, M. J. Joyce, A. Lavietes, R. Plenteda, F. D. Cave, H. Parker, A. Jones, V. Astromskas, Real-time capabilities of a digital analyzer for mixed-field assay using scintillation detectors, IEEE Trans. Nucl. Sci. 64. doi:10.1109/TNS.2017.2654512.